Meteoritics & Planetary Science 40, Nr 11, 1581–1598 (2005)
Abstract available online at http://meteoritics.org

Petrology of the Yamato nakhlites

N. IMAE[1, 2*], Y. IKEDA[3], and H. KOJIMA[1, 2]

[1]Antarctic Meteorite Research Center, National Institute of Polar Research, 9-10, Kaga 1-chome, Itabashi-ku, Tokyo 173-8515, Japan
[2]Department of Polar Science, School of Multidisciplinary Science, The Graduate University for Advanced Studies, 9-10, Kaga 1-chome, Itabashi-ku, Tokyo 173-8515, Japan
[3]Department of Material and Biological Sciences, Ibaraki University, Mito 310-8512, Japan
*Corresponding author. E-mail: imae@nipr.ac.jp

(Received 10 May 2004; revision accepted 12 July 2005)

Abstract–The Yamato nakhlites, Y-000593, Y-000749, and Y-000802, were recovered in 2000 from the bare icefield around the Yamato mountains in Antarctica, consisting of three independent specimens with black fusion crusts. They are paired cumulate clinopyroxenites. We obtained the intercumulus melt composition of the Yamato nakhlites and here call it the Yamato intercumulus melt (YIM). The YIM crystallized to form the augite rims, the olivine rims and the mesostasis phases in the cumulates. The augite rims consist of two layers: inner and outer. The crystallization of the inner rim drove the interstitial melt into the plagioclase liquidus field. Subsequently, the residual melt crystallized pigeonites and plagioclase to form the outer rims and the mesostasis.

Three types of inclusions were identified in olivine phenocrysts: rounded vitrophyric, angular vitrophyric, and monomineralic augite inclusions. The monomineralic augite inclusions are common and may have been captured by growing olivine phenocrysts. The rounded vitrophyric inclusions are rare and may represent the composition of middle-stage melts, whereas the angular vitrophyric inclusions seem to have been derived from fractionated late-stage melts. Glass inclusions occur in close association with titanomagnetite and ferroan augite halo in phenocryst core augites and the assemblages may be magmatic inclusions in augites. We compared the YIM with compositions of magmatic inclusions in olivine and augite. The composition of magmatic inclusions in augite is similar to the YIM.

Phenocrystic olivines contain exsolution lamellae, augite-magnetite aggregates, and symplectites in the cores. The symplectites often occur at the boundaries between olivine and augite grains. The aggregates, symplectite and lamellae formed by exsolution from the host olivine at magmatic temperatures.

We present a formational scenario for nakhlites as follows: (1) accumulation of augite, olivine, and titanomagnetite phenocrysts took place on the floor of a magma chamber; (2) olivine exsolved augite and magnetite as augite-magnetite aggregates, symplectites and lamellae; (3) the overgrowth on olivine phenocrysts formed their rims, and the inner rims crystallized on augite phenocryst cores; and finally, (4) the outer rim formed surrounding the inner rims of augite phenocrysts, and plagioclase and minor minerals crystallized to form mesostasis under a rapid cooling condition, probably in a lava flow or a sill.

INTRODUCTION

Nakhlites are petrographically classified as clinopyroxenites (e.g., McSween 1985), and they include seven meteorites: Nakhla, Governador Valadares, Lafayette, NWA 817, NWA 998, the Yamato nakhlites (Y-000593, Y-000749, and Y-000802) and MIL 03346. Many mineralogical-petrological studies of nakhlites have been published for Nakhla, Governador Valadares, and Lafayette (e.g., Prior 1912; Bunch and Reid 1975; Burrangato et al. 1975; Treiman 1986; Longhi and Pan 1989; Treiman 1990; Longhi 1991; Harvey and McSween 1992a, 1992b; Treiman 1993; Friedman Lentz et al. 1999), for NWA 817 (e.g., Sautter et al. 2002), for NWA 998 (e.g., Irving et al. 2002; Bridges et al. 2004), for the Yamato nakhlites (e.g., Misawa et al. 2003; papers in *Antarctic Meteorite Research* 16), and for MIL 03346 (e.g., McKay and Schwandt 2005; abstracts for the 36th Lunar and Planetary Science Conference). However,

the detailed magmatic processes for the nakhlites have not been fully clarified. In this study, we present the petrology of new Yamato nakhlites (Y-000593, Y-000749, and Y-000802) and try to clarify the details of the crystallization process of the nakhlite magma.

As all nakhlites are cumulates, the bulk composition of nakhlites does not represent their melt composition. There are three methods for estimation of the melt composition. One is to estimate the trapped compositions from magmatic inclusions in olivine phenocrysts (Harvey and McSween 1992b; Treiman 1993) and augite phenocrysts (Varela et al. 2001). The second is to determine the composition of intercumulus melt by the subtraction of cumulate phases from the whole rock composition (Treiman 1986). The third is to find the consistent melt composition from results of isothermal heating experiments (Longhi and Pan 1989; Kaneda et al. 1998; Treiman and Goodrich 2001). In this study, we determined the chemical compositions of the intercumulus melt of the Yamato nakhlites by the second method, and compared it with the melt compositions obtained by the first method.

The olivine phenocrysts in the Yamato nakhlites contain augite-magnetite exsolution lamellae in the cores, and augite-magnetite symplectites at the boundaries between olivine and augite grains, suggesting that the Yamato nakhlites might have cooled slowly. On the other hand, the Yamato nakhlites contain fine-grained intercumulus mesostasis between olivine and augite phenocrysts and glasses in trapped melt in olivine and augite phenocrysts, suggesting that they cooled rapidly. We will discuss the apparent contradiction of cooling rates for the Yamato nakhlites and present a formational scenario for the Yamato nakhlites.

ANALYTICAL METHODS

Polished thin sections of Y-000593 (61, 62, 67-1, and 63-2), Y-000749 (1-1 and 1-3), and Y-000802 (20-1) were used for petrographical observation under an optical microscope (Fig. 1a). Compositions of minerals were determined using two electron probe microanalyzers (JXA-8800 and JXA-8200 at NIPR, and JXA-733 at Ibaraki University). The accelerating voltage and beam currents were 15 kV and about 5–10 nA, respectively. For the analysis of glasses in augite and olivine phenocrysts, a defocused beam of 10 μm in diameter with a beam current of 3 nA and counting time of 10 sec was used. The Bence and Albee corrections were applied for silicates and oxides, and the standard ZAF corrections for sulfides. The bulk composition of mesostasis was obtained using the defocused beam of an electron probe microanalyzer with a beam 50 μm in diameter, and was corrected by the method of Ikeda (1980). Modal abundances of mineral and glass phases in rounded vitrophyric inclusions were determined using the method of Imae et al. (2003). Similarly, the abundance of cumulate cores of augite phenocrysts was determined using backscattered electron images.

PETROLOGY

The Yamato nakhlites are unbrecciated cumulate rocks and mainly consist of euhedral coarse-grained crystals of augite set in a fine-grained mesostasis (Figs. 1a and 1b). The companion paper (Imae et al. 2003) describes mineralogical and petrographic features of the Yamato nakhlites. Augite is a main cumulate phase, and olivines and titanomagnetites also occur as minor cumulate phases in the Yamato nakhlites. Mean modal abundances of the Yamato nakhlites (vol%) are pyroxene phenocrysts 77%, olivine phenocrysts 12%, titanomagnetite microphenocrysts 1%, and mesostasis 10%. These modal abundances are similar to those for other nakhlites, but the abundance of mesostasis in the Yamato nakhlites is somewhat higher than those of Nakhla, Governador Valadares, and Lafayette, and is somewhat lower than that of NWA 817 (Imae et al. 2003). Bulk compositions of Y-000593 and Y-000749 obtained by wet chemical analyses are very similar to each other, supporting their pairing (Imae et al. 2003), and the simply averaged bulk composition is listed in Table 1. This roughly resembles other nakhlites in bulk composition, although the Al_2O_3 content is somewhat higher (Imae et al. 2003).

Pyroxene Phenocrysts

Phenocrystic augites have chemically homogeneous cores ($En_{36}Fs_{25}Wo_{39}$) (Figs. 2 and 3), and the compositions of pyroxenes are summarized in Table 2. Rims of augite phenocrysts have thicknesses of 40–100 μm and a gradual compositional zoning toward ferroan pyroxenes (Fig. 3). The augite rims in contact with other cumulate grains such as augite, olivine, or titanomagnetite, are thinner or absent, but augite rims in contact with mesostasis are thicker and richer in Fe. Average modal abundances of cumulate augite cores and rims are 61.1 vol% and 15.9 vol%, respectively.

Based on the abrupt change of the Al_2O_3 content, the rims are divided into two zones: the inner and outer rims (Fig. 3). The Al_2O_3 contents of the inner rim increase outward from 0.5 wt% to 2–3 wt% (Fig. 3), and those of the outer rims decrease abruptly down to 0.4–0.5 wt% (Fig. 3). Wo contents of the inner rim augite are nearly the same as those of the core augite, but the Wo contents of the outer rim augite decrease outwards. The outermost pyroxenes are pigeonite. The inner rim is ~70 μm thick, and the outer rim is generally thinner than a few tens of μm.

Magmatic Inclusions in Augite Phenocryst Cores

Small Si-rich glass inclusions are common in core augite (Table 3; Fig. 1c), and these are similar to the small Si-rich glass inclusions described in Nakhla by Varela et al. (2001). They are magmatic inclusions that were trapped in core augites. Inclusions of titanomagnetite smaller than a few tens of μm in size usually occur in close association with the Si-

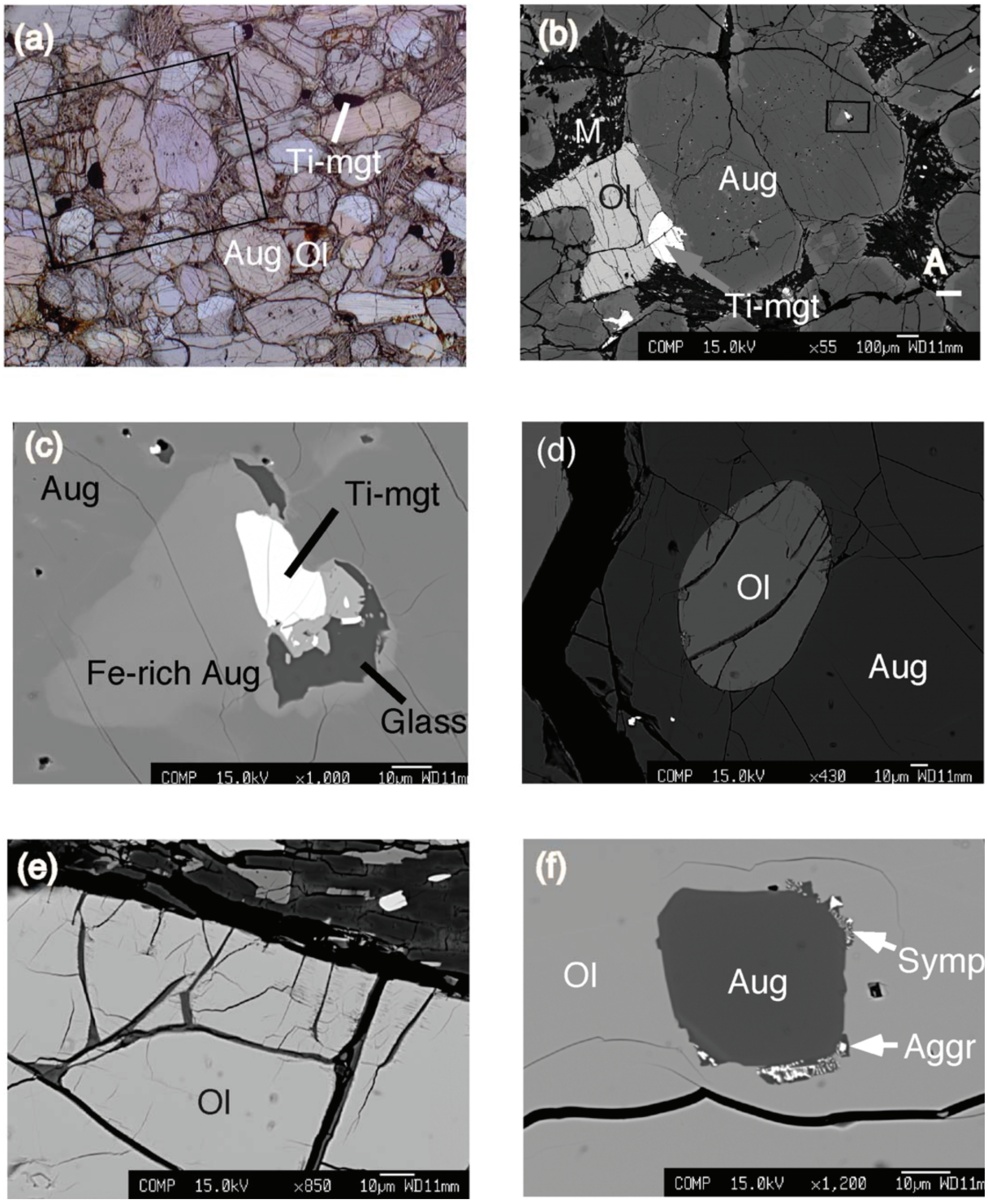

Fig. 1. Representative images in Y-000593, Y-000749, and Y-000802. Aggr: augite-magnetite aggregate; Alk-fel: alkali feldspar; Alt: altered phase; Ap: apatite; Aug: augite; Gl: glass; Idd: iddingsite; Lam: exsolution lamellae; M: mesostasis; Ol: olivine; Pig: pigeonite; Pl: plagioclase; Si: tridymite; Sympl: symplectite; Ti-mgt: titanomagnetite. a) A polished thin section (Y-000593, 61) photomicrograph with transmitted light. The side is 5 mm. b) Y-000593, 61. Enlarged view of the square in Fig. 1a under the backscattered electron image (BEI). The zoning profile indicated as A is shown in Fig. 3. c) Y-000593, 61. BEI enlarged view of the square in Fig. 1b. Inclusions of glass, titanomagnetite and ferroan augite halo in an augite phenocryst core. The glass is always surrounded by a ferroan halo. d) BEI of a rounded monocrystalline olivine inclusion in an augite phenocryst in Y-000749,1-3. e) BEI of a weathered portion in an olivine phenocryst. f) Y-000593,61. BEI of an augite inclusion in an olivine phenocryst. Symplectite seen in the interface between the augite inclusion and the host olivine. Y-000593,61. An olivine phenocryst with subhedral shape.

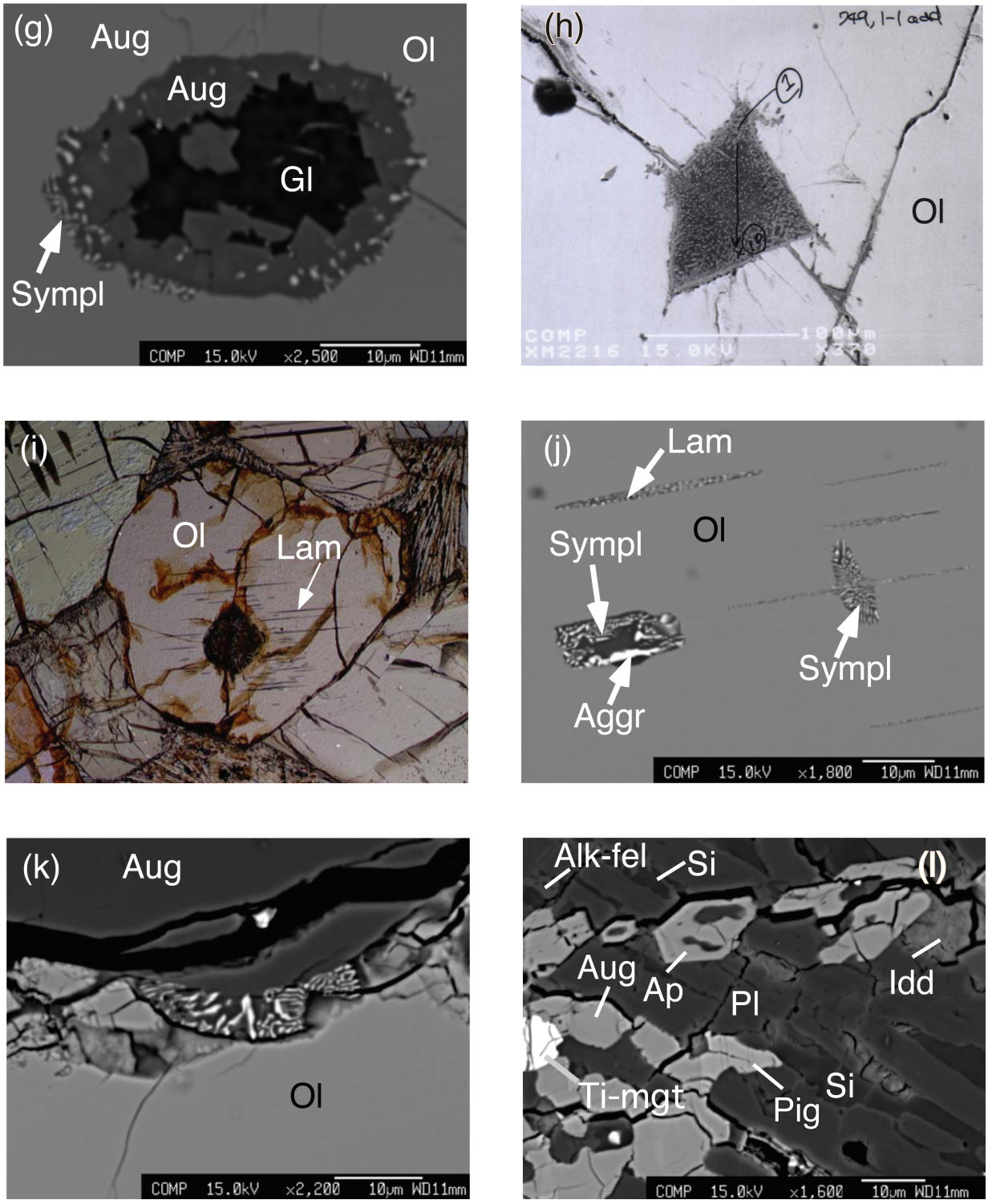

Fig. 1. *Continued*. Representative images in Y-000593, Y-000749, and Y-000802. Aggr: augite-magnetite aggregate; Alk-fel: alkali feldspar; Alt: altered phase; Ap: apatite; Aug: augite; Gl: glass; Idd: iddingsite; Lam: exsolution lamellae; M: mesostasis; Ol: olivine; Pig: pigeonite; Pl: plagioclase; Si: tridymite; Sympl: symplectite; and Ti-mgt: titanomagnetite. g) BEI of a rounded vitrophric inclusion (RVI-5) in Y-000749, 1-3. h) BEI of an angular vitrophyric inclusion in an olivine phenocryst in Y-000749,1-1. i) Exsolution lamellae in an olivine with transmitted light. Y-000802,20-1. The side is 0.6 mm. j) BEI of a symplectite in lamella and augite-magnetite aggregate in an olivine phenocryst in Y-000593, 61. k) BEI of symplectites occurring at the interface between olivine phenocryst and augite phenocryst in Y-000593, 61. l) BEI of an enlarged mesostasis mainly consisting of plagioclase in Y-000593, 61. Other constituting minerals are plagioclase, alkali feldspar, tridymite, titanomagnetite, augite, pigeonite, augite, apatite, and iddingsite. The pigeonite exsolves lamellae.

Table 1. Bulk chemical compositions (wt%) of nakhlites, inclusions, and mesostasis.

	Average bulk[a]	Bulk of AVI[b]	Bulk of inclusion[c]	Mesostasis[d]
SiO_2	48.35	60.94	47.10	66.74
TiO_2	0.47	0.88	1.93	0.18
Al_2O_3	1.96	12.69	6.69	14.57
Fe_2O_3	2.04	–	–	–
FeO	19.51	8.83	24.15	6.93
MnO	0.59	0.13	0.44	0.10
MgO	11.09	1.94	5.82	0.88
CaO	14.90	7.44	11.35	5.66
Na_2O	0.66	4.06	1.83	3.68
K_2O	0.17	0.71	0.30	1.26
H_2O (–)	0.03	–	–	–
H_2O (+)	0.00	–	–	–
P_2O_5	0.21	–	0.24	–
Cr_2O_3	0.26	0.00	0.15	0.00
FeS	0.08	–	–	–
NiO	–	–	–	–
Total	100.32	97.62	100.00	100.00

[a]Average bulk composition of Y-000593 and Y-000749, analyzed by H. Haramura.
[b]Bulk of angular vitrophyric inclusion (AVI) averaged 10 point analyses.
[c]Averaged 4 sets of inclusions consisting of glass, titanomagnetite, and Fe-rich augite halo in augite phenocryst cores.
[d]Bulk of mesostasis by broad beam analyses of 50 μm, averaged from 3 mesostases.

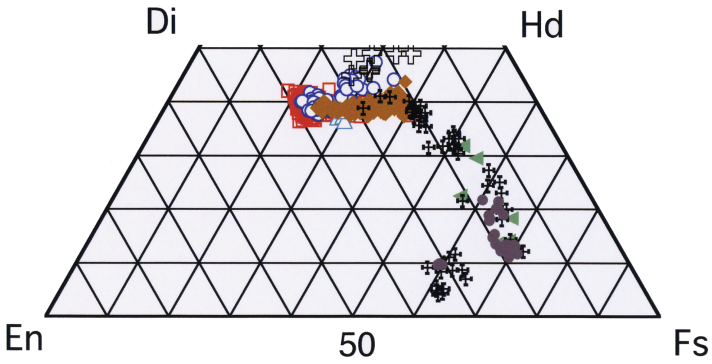

Fig. 2. Compositional variation of pyroxenes in three Yamato nakhlites (Y-000593, Y-000749, and Y-000802). Red open square: phenocryst cores of augites. Blue open circle: augite inclusions in olivines. Light blue open triangle: halos augite contact with titanomagnetite. Brown closed square: inner rims of augite phenocrysts. Green closed triangle: outer rims of augite phenocrysts. Cross: pyroxenes in mesostasis. Black closed circle: pigeonites in mesostasis. Open cross: augites in a rounded vitrophyric inclusion in an olivine phenocryst. The compositions of augite core are concentrated around the area of $En_{40–36}Fs_{25}Wo_{39}$. Rims of augite grains rapidly become ferroan, resulting in chemical zoning in rim region as shown in Fig. 3. Rim is divided into two based on Al_2O_3 (wt%) content: inner rim and outer rim as shown in Fig. 3. Wo content of the inner rim is kept to be identical with core. The Wo content at the outer rim drastically decreases, suggesting the formation of pigeonite. Most pyroxenes in mesostasis are Ca-poor and they are subcalcic augite and pigeonite.

rich glass inclusions (Fig. 1c). Ferroan augite halos commonly surround Si-rich glass inclusions (Table 2; Fig. 1c). The FeO and Al_2O_3 contents of the halos are discontinuous between magnesian augite phenocryst core (Fs = 22 mol%, Al_2O_3 = 0.7 wt%) and the ferroan augite halo (Fs = 37 mol%, Al_2O_3 = 1.4 wt%). The FeO, Al_2O_3, TiO_2, and Na_2O contents of the ferroan augite halos rapidly increase up to 56 mol%, 4 wt%, 0.85 wt%, and 0.6 wt%, respectively, within 5 μm from the boundaries between Si-rich glass inclusion and the ferroan augite halo. Although the CaO and MgO contents of the ferroan augite halo are discontinuous at the boundaries between the magnesian core augite (Wo = 40 mol%, En = 35 mol%) and the ferroan augite halo (Wo = 35 mol%, En = 25 mol%), these contents gradually decrease towards the Si-rich glass inclusion up to Wo = 22 mol% and En = 22 mol%.

Olivine Phenocrysts

Olivine phenocrysts usually have subhedral to anhedral shapes with diameters up to 0.8 mm. Core olivines are relatively magnesian (58 ≤ Fa ≤ ~70) and the rims are ferroan (~70 ≤ Fa ≤ 78) (Table 3). The CaO content decreases from core (~0.5 wt%) to rim (~0.1 wt%). More ferroan olivines

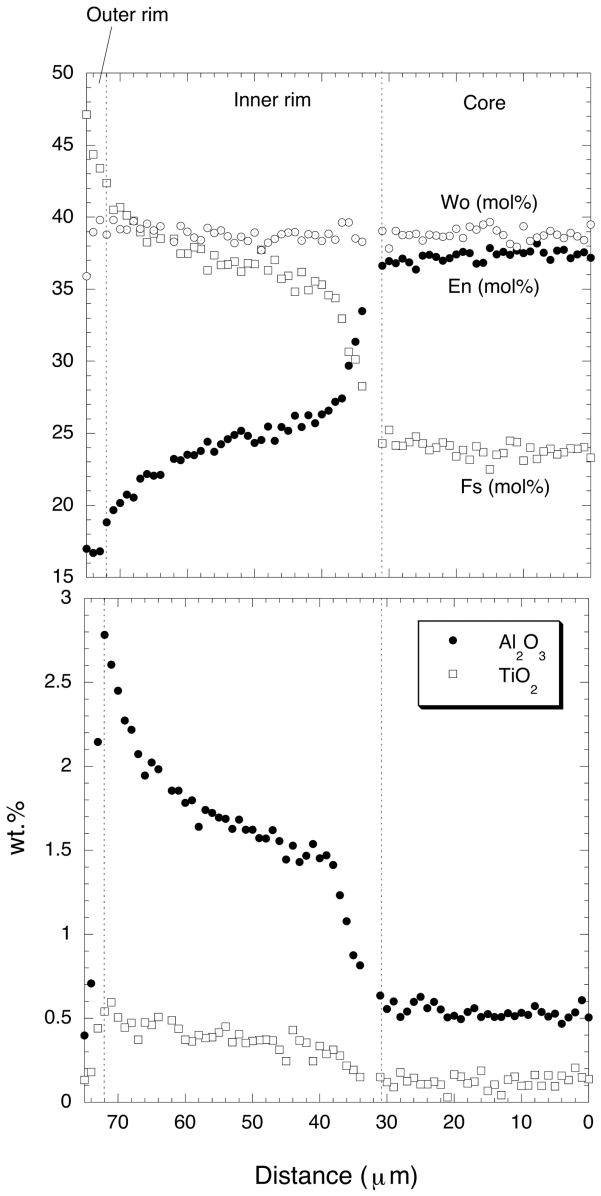

Fig. 3. Zoning profile of a cumulus augite contact with mesostasis. Y-000593,61. Inner rim (42 μm) is thicker than outer rim (2 μm). Y-000593,61. The composition of En and Al_2O_3 at the interface between core and inner rim changes drastically. The discontinuity in Al_2O_3 in the rim is clearly shown in the zoning.

($Fa_{83–87}$) occur at the outermost rims in contact with mesostasis, while olivine in contact with augite is less ferroan. The MnO content is ~1 wt%. A rounded monocrystalline olivine inclusion occurs in a phenocryst core augite, and the compositions are Fa_{62} in the inclusion core and Fa_{66} in the inclusion rim (Fig. 1d).

Rims and fractures in olivines are usually weathered (Fig. 1e), and hydrous mineral phases (iddingsite) occur there (Imae et al. 2003; Noguchi et al. 2003). The chemical composition of iddingsite is shown in Table 3, and the hydrous minerals had formed by the aqueous reaction between olivine and fluids on Martian surface and/or terrestrial Antarctica (Imae et al. 2003; Noguchi et al. 2003). Central portions of weathered veins with thicknesses of several μm are Si-rich, but the peripheral portions of the veins with thickness of several m are Fe-rich, accompanying a comb structure (Fig. 1e; Table 3).

Inclusions in Olivine

Olivines often contain three types of inclusions, sizes of which are several tens of μm up to 100 μm. Although most of these inclusions are a monomineralic augite type (Fig. 1f), two types of vitrophyric inclusions, rounded (Fig. 1g) and angular (Fig. 1h) occur. The latter two types are magmatic inclusions. The rounded vitrophyric inclusions are very rare, and have a rim consisting of fine-grained crystals of augite and titanomagnetite with the thickness of ~3 μm (Fig. 1g). The cores of the rounded vitrophyric inclusions consist mainly of augite and glass with minor magnetites. The Wo, Al_2O_3 and TiO_2 contents of augites in rounded vitrophyric inclusions are slightly higher than those of phenocrystic core augites (Fig. 2; Table 2). Rounded vitrophyric inclusions in Nakhla and Governador Valadares have been described by Harvey and McSween (1992b) and Treiman (1993), and they are very similar to those in the Yamato nakhlites. Although the CaO content of olivine decreases within 60–70 μm toward the vitrophyric inclusion, the Fa content is unaffected by the existence of the inclusion (Fig. 4). Angular vitrophyric inclusions (Fig. 1h) consist of fine-grained phases (Table 1), and this is the first report of the occurrence of this type among all nakhlites.

Exsolution Lamellae, Symplectites, and Augite-Magnetite Aggregate in Olivine

Olivines in the Yamato nakhlites contain exsolution lamellae, which are observed under a polarizing optical microscope (Fig. 1i) and in backscattered electron images (Fig. 1j). Each exsolution lamella shows flattened lens shape, 30–40 μm in length, and less than 2 μm in thickness. Usually, the lamellae are not homogeneously distributed within a host olivine grain, but are localized in some portions of the olivine grain (Fig. 1i). The lamellae have a preferred orientation with crystallographic axes of the host olivine, perpendicular to (100), and the extinction position of the host olivine crystal coincides with the elongated direction of lamellae. They consist of two phases, although these phases are too fine-grained to determine the mineral compositions by an electron-probe microanalyzer. The lamellae structure of Y-000593 is similar in appearance to those observed in Nakhla (Mikouchi et al. 2000) and Chassigny (Greshake et al. 1998). Mikouchi et al. (2000) reported that the two phases of lamellae in Nakhla are magnetite and augite.

Table 2. Average chemical composition of pyroxenes (wt%) and structural formulae based on 24 oxygens.

	Y-000593,61	Y-000593,61	Y-000593,61	Y-000593,61	Y-000593,61	Y-000593,61	Y-000593,61	Y-000593,61	Y-000802,20-1	Y-000802,20-1
Occurrence	Phenocrysts core augite	Inner rim	Outer rim	Augite in mesostasis	Ca-poor px in mesostasis	Halo around titanomagnetite in augite	Magnesian augite in symplectite	Ferroan augite in symplectite	Augite in vitrophyric inclusion in an olivine	Augite inclusions in olivines
Number of analyses	177	18	1	1	5	1	1	1	8	11
SiO_2	51.44	49.70	47.82	49.47	47.95	47.52	51.26	47.54	45.32	51.34
TiO_2	0.25	0.35	0.30	0.19	0.36	0.29	0.03	1.61	1.85	0.24
Al_2O_3	0.85	1.38	0.51	0.50	0.67	4.03	0.73	0.52	5.52	0.78
Cr_2O_3	0.33	0.10	0.03	0.01	0.01	0.03	0.05	0.08	0.04	0.41
NiO	0.02	0.02	0.00	0.01	0.01	–	0.00	0.04	0.02	0.02
FeO	15.03	20.76	37.45	24.03	34.88	23.58	13.21	22.98	16.98	14.28
MnO	0.43	0.51	1.08	0.77	0.89	0.53	0.33	0.65	0.41	0.42
MgO	12.39	8.72	4.70	6.25	5.45	6.58	11.17	7.66	7.23	12.48
CaO	18.63	17.97	8.03	17.71	9.08	15.80	21.78	17.38	20.83	18.58
Na_2O	0.23	0.25	0.13	0.19	0.15	0.48	0.18	0.26	0.32	0.20
K_2O	0.01	0.01	0.00	0.01	0.01	0.03	0.01	0.01	0.05	0.00
P_2O_5	0.04	0.02	0.00	0.03	0.01	0.07	0.00	0.05	0.58	0.01
Total	99.63	99.78	100.04	99.16	99.47	98.94	98.75	98.78	99.14	98.77
Si	7.88	7.81	7.91	7.95	7.90	7.59	7.91	7.67	7.14	7.90
Ti	0.03	0.04	0.04	0.02	0.04	0.03	0.00	0.20	0.22	0.03
Al	0.15	0.26	0.10	0.10	0.13	0.76	0.13	0.10	1.02	0.14
Cr	0.04	0.01	0.00	0.00	0.00	0.00	0.00	0.01	0.01	0.05
Ni	0.00	0.00	0.00	0.00	0.00	–	0.00	0.00	0.00	0.00
Fe	1.92	2.73	5.18	3.23	4.81	3.15	1.70	3.10	2.24	1.84
Mn	0.06	0.07	0.15	0.11	0.12	0.07	0.04	0.09	0.05	0.05
Mg	2.83	2.04	1.16	1.50	1.34	1.57	2.57	1.84	1.70	2.86
Ca	3.05	3.02	1.42	3.05	1.60	2.71	3.60	3.01	3.51	3.06
Na	0.07	0.08	0.04	0.06	0.05	0.15	0.05	0.08	0.10	0.06
K	0.00	0.00	0.00	0.00	0.00	0.01	0.00	0.00	0.01	0.00
P	0.00	0.00	0.00	0.00	0.00	0.01	0.00	0.01	0.08	0.00
Total	16.03	16.05	16.01	16.01	16.00	16.05	16.00	16.11	16.07	16.01
En (mol%)	36.16	26.11	14.92	19.27	17.22	21.13	32.62	23.17	22.79	36.87
Fs (mol%)	24.72	35.11	66.75	41.52	62.03	42.40	21.65	39.03	30.02	23.66
Wo (mol%)	39.12	38.79	18.33	39.21	20.75	36.47	45.73	37.80	47.19	39.47

Table 3. Chemical compositions of representative minerals and glasses except pyroxenes in the Yamato nakhlite (wt%) and structural formulae based on 24 oxygens.

	Y-000593,61	Y-000593,61	Y-000593,61	Y-000593,61	Y-000593,61	Y-000593,61	Y-000593,61	Y-000593,61
Mineral name	Olivine	Olivine	Plagioclase	Orthoclase	Titanomagnetite	Ilmenite	Si-rich iddingsite	Fe-rich iddingsite
Occurrence	Core	Rim	Mesostasis	Mesostasis	Phenocryst	Exsolution		
SiO_2	32.27	31.69	58.46	66.42	0.04	0.01	52.00	24.75
TiO_2	0.00	0.03	0.14	0.17	15.92	52.02	0.04	0.02
Al_2O_3	0.02	0.00	24.29	19.76	2.57		1.15	0.07
Cr_2O_3	0.06	0.00	0.00	0.10	0.80	0.09	0.00	0.05
NiO	0.05	0.00	0.01	0.00	0.02	0.02	0.02	–
FeO	53.11	56.16	1.29	0.51	34.58 (calc)	46.27	26.25	57.40
Fe_2O_3	–	–	–	–	44.98 (calc)	–	–	–
MnO	0.94	1.10	0.00	0.10	0.38	0.65	0.51	1.74
MgO	12.79	10.27	0.05	0.00	0.49	1.25	4.80	4.18
CaO	0.43	0.14	7.30	0.65	0.00	0.08	0.04	0.38
Na_2O	0.00	0.03	6.70	3.71	0.03	0.00	0.04	0.47
K_2O	0.00	0.00	0.57	10.45	0.00	0.00	0.16	0.04
P_2O_5	0.02	0.00	0.23	0.00	0.00	0.00	0.00	0.06
SO_3	–	–	–	–	–	–	–	1.08
Total	99.70	99.40	99.00	101.90	99.81	100.39	85.02	90.24
Si	5.98	6.00	7.95	8.87	0.01	0.00	9.19	5.45
Ti	0.00	0.00	0.01	0.02	2.60	7.85	0.01	0.00
Al	0.00	0.00	3.89	3.11	0.66	0.00	0.24	0.02
Cr	0.01	0.00	0.00	0.01	0.14	0.01	0.00	0.01
Ni	0.01	0.00	0.00	0.00	0.00	0.00	0.00	0.01
Fe	8.23	8.89	0.15	0.06	6.29	7.77	3.88	10.58
Fe^{3+}	–	–	–	–	7.37	–	–	–
Mn	0.15	0.18	0.00	0.01	0.07	0.11	0.08	0.32
Mg	3.53	2.90	0.01	0.00	0.16	0.37	1.26	1.37
Ca	0.09	0.03	1.06	0.09	0.00	0.02	0.01	0.09
Na	0.00	0.01	1.77	0.96	0.01	0.00	0.01	0.20
K	0.00	0.00	0.10	1.78	0.00	0.00	0.04	0.01
P	0.00	0.00	0.03	0.00	0.00	0.00	0.00	0.01
S	–	–	–	–	–	–	–	0.18
Total	18.00	18.01	14.97	14.91	17.32	16.14	14.71	18.25
	$Fa_{70.0}$	$Fa_{75.4}$	$Ab_{65.4}An_{31.1}Or_{3.5}$	$Ab_{33.9}An_{3.2}Or_{62.8}$	$Mgt_{58.5}Usp_{41.5}$			

Table 3. *Continued*. Chemical compositions of representative minerals and glasses except pyroxenes in the Yamato nakhlite (wt%) and structural formulae based on 24 oxygens.

	Y-000593,61	Y-000593,61	Y-000802,20-1	Y-000749,1-3	Y-000749,1-3	Y-000749,1-3	Y-000749,1-3		Y-000593,61
Mineral name	Plagioclase	Alkali feldspar	Glass (9 averaged)	Glass	Glass in augite phenocryst	Tridymite	Magnetite		Pyrrhotite
Occurrence	Mesostasis	Mesostasis	RVI-1	RVI-5	Core	Mesostasis	Mesostasis		Mesostasis
SiO_2	61.36	65.34	66.15	68.13	69.86	98.22	0.00	Si	0.07
TiO_2	0.03	0.09	0.20	0.00	0.01	0.02	0.16	Ti	0.00
Al_2O_3	24.51	20.23	14.08	20.28	17.46	0.47	1.06	Al	0.00
$Cr2_2O_3$	0.02	0.00	0.00	0.00	0.00	0.00	0.66	Cr	0.00
NiO	–	–	0.02	0.00	–	–	0.00	Ni	0.00
FeO	0.81	0.37	2.31	1.52	1.24	0.55	91.09	Fe	59.52
Fe_2O_3	–	–		–	–	–	–	S	39.33
MnO	0.00	0.00	0.06	0.00	0.09	0.00	0.24	Mn	0.00
MgO	0.04	0.00	0.78	0.04	0.16	0.00	0.03	Mg	0.01
CaO	5.02	0.90	4.41	0.64	0.93	0.00	0.23	Ca	0.00
Na_2O	8.13	5.31	2.13	7.33	6.50	0.17	0.04	Na	0.00
K_2O	0.88	8.53	4.78	2.06	2.74	0.01	0.01	K	0.00
P_2O_5	0.10	0.00	1.80	0.00	0.14	–	–	P	0.00
Cl	–	–		0.33	–	–	0.01	Co	0.17
Total	100.90	100.77	96.72	100.33	99.13	99.44	93.52	Total	99.11
Si	8.14	8.80	8.68	8.96	9.26	11.91	0.00		
Ti	0.00	0.01	0.09	0.00	0.00	0.00	0.04		
Al	3.83	3.21	2.13	3.14	2.73	0.07	0.38		
Cr	0.00	0.00	0.00	0.00	0.00	0.00	0.16		
Fe	0.09	0.04	1.05	0.17	0.14	0.06	22.96		
Mn	0.00	0.00	0.02	0.00	0.01	0.00	0.06		
Mg	0.01	0.00	0.41	0.01	0.03	0.00	0.01		
Ca	0.71	0.13	1.14	0.09	0.13	0.00	0.07		
Na	2.09	1.39	1.12	1.87	1.67	0.04	0.02		
K	0.15	1.46	0.13	0.35	0.46	0.00	0.00		
P	0.01	0.00	0.01	–	–	–	–		
Total	15.04	15.04	14.78	14.58	14.44	12.08	23.71		
	$Ab7_{0.81}An_{24.1}Or_{5.1}$	$Ab_{46.5}An_{4.3}Or_{49.1}$							$Fe_{0.87}S$

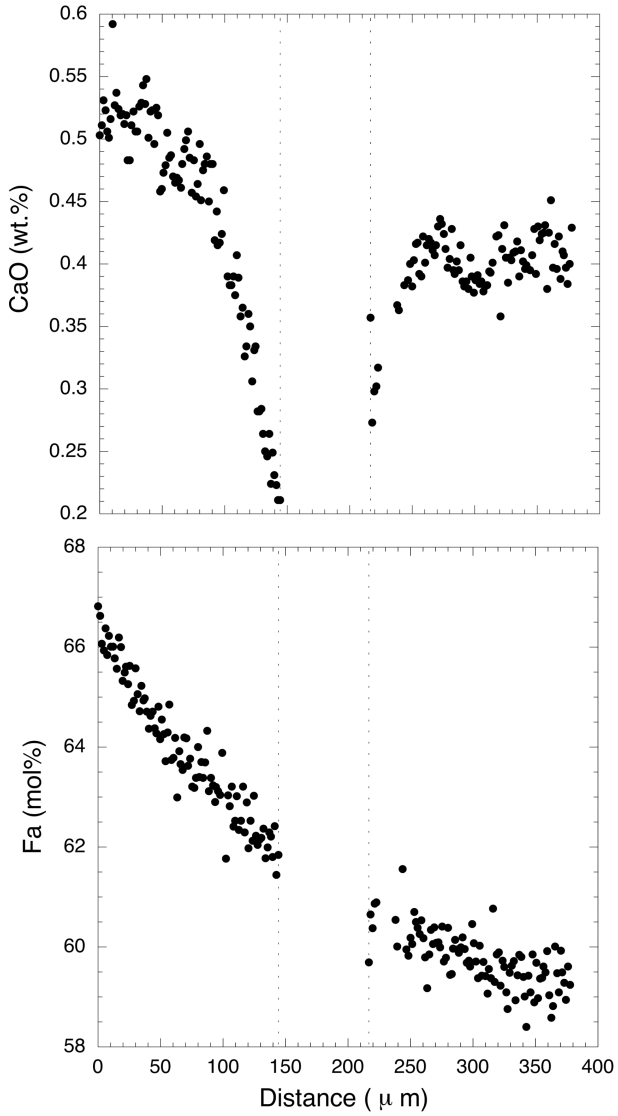

Fig. 4. CaO and Fa zoning profile surrounding a rounded vitrophyric inclusion in an olivine phenocryst core in Y-000802,20-1.

Intergrowths of augite and magnetite showing symplectic structures are found at the boundaries between olivine and augite phenocrysts (Figs. 1f and 1k). The constituent phases were determined by an electron probe microanalyzer (Tables 2 and 3). Though the compositions of augites in the symplectites are mostly similar to the phenocryst core augite, more ferroan augites than the phenocryst core augite also occur. The symplectites are firmly fixed to the augite (Fig. 1k), indicating that the surface of augite phenocrysts worked as nucleation site for symplectite formation. Concave outlines of symplectites against olivine (Fig. 1k) suggest that olivine exsolved augite and magnetite components to form symplectites. These symplectites do not seem to occur in any specific crystallographic orientation of olivines. Symplectites rarely occur together with lamellae within olivine phenocrysts (Fig. 1j).

Augite-magnetite aggregates have square shapes and are coarser-grained than symplectites (Figs. 1f and 1j). They have identical compositions of magnetite and augite with those of symplectites. They often coexist with symplectites or occur independently in olivine phenocrysts.

Titanomagnetite Micro-Phenocrysts

Micro-phenocrysts of titanomagnetite (Fig. 1a) are subhedral to anhedral with diameters of about 100–200 μm, and include ilmenite exsolution lamellae of ~10 μm in width. The titanomagnetite has the chemical composition mainly between two end components, pure magnetite (Fe_3O_4) and ulvöspinel (Fe_2TiO_4), and is in the range of 32–68 mol% magnetite and of 32–68 mol% ulvöspinel. The Al_2O_3 and Cr_2O_3 contents of titanomagnetites are low (Table 3). The ilmenites often associate with titanomagnetites, and have a stoichiometric composition (Table 3).

Mesostasis

Mesostasis consists mainly of lath-shaped plagioclase with sodic compositions of $Ab_{60.3–68.1}An_{22.0–36.3}Or_{2.7–15.7}$ (Fig. 1l). Other mesostasis minerals are K-feldspar ($Ab_{33.9}An_{3.2}Or_{62.8}$), titanomagnetite, ferroan augite, pigeonite, fayalitic olivine ($Fa_{\sim 85}$), pyrrhotite ($Fe_{0.86–0.91}S$), Cl-apatite, and a silica mineral (Imae et al. 2003) (Fig. 1l). Iddingsites sometimes occur in mesostasis (Fig. 1l). Pigeonite in mesostasis has exsolution lamellae (Fig. 1l). The composition of pigeonite in the mesostasis overlaps in composition with that of the outermost rims of pyroxene phenocrysts (Fig. 2; Table 2), suggesting that pigeonites crystallized both in outer rims and in mesostasis. The silica mineral was identified to be tridymite by X-ray analyses using a Gandolfi camera (Imae et al. 2003).

IGNEOUS PETROGENESIS FOR THE YAMATO NAKHLITES

Yamato Intercumulus Melt (YIM) Composition: Mass Balance Calculation

Phenocryst core augite with homogeneous composition is a cumulus phase, while phenocryst rim augite is an overgrowth phase from intercumulus melt. Micro-phenocryst titanomagnetite is another cumulus phase. Olivine grains in the Yamato nakhlites are phenocrystic and some fractions of the olivine can be a cumulus phase. However, cumulus components of olivine phenocrysts are uncertain, and the cumulate fraction k [k = (mode of cumulus olivine)/(mode of phenocrystic olivine) = 0 to 1] of olivine phenocrysts was considered for the mass balance calculation. All micro-phenocrystic titanomagnetite is assumed to be a cumulus phase.

We calculate the intercumulus melt composition by

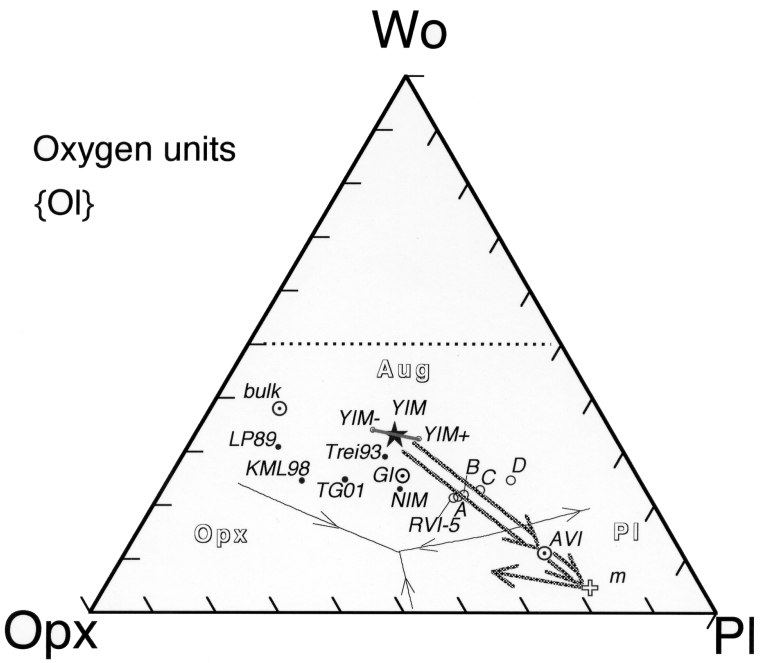

Fig. 5. A pseudoternary phase diagram of Wo-Opx-Pl showing the crystallization from the intercumulus melt of the Yamato nakhlites (YIM) derived from the mass balance calculation resulting in the formation of the inner and outer rims of pyroxene phenocryst and the mesostasis of plagioclase and Ca-poor pyroxene. Wo: wollastonite; Opx: orthopyroxene; Pl: plagioclase; Aug: augite. The crystallization paths are indicated as thick arrows. YIM-: the estimated error for YIM (mode of augite core =58.1 vol% and mode of cumulate olivine =10.7 vol%). YIM+: the estimated error for YIM (mode of augite core =64.1 vol% and mode of cumulate olivine =7.6 vol%). m: averaged bulk chemical composition of mesostasis. bulk: Average bulk of the Yamato nakhlites. Gl: Inclusion consisting of glass, titanomagnetite, and ferroan augite halo in augite phenocryst cores in the Yamato nakhlites. AVI: averaged compositions of an angular vitrophyric inclusion. RVI-5: the bulk composition of a rounded vitrophric inclusion before the Fe/Mg correction. A: RVI-5 and wall olivine 10 vol% with the correction of the Fe/Mg partitioning in equilibrium with Fa_{50}. B: RVI-5 and wall olivine 20 vol% with the correction of the Fe/Mg partitioning in equilibrium with Fa_{50}. C: RVI-5 and wall olivine 30 vol% with the correction of the Fe/Mg partitioning in equilibrium with Fa_{50}. D: RVI-5 and wall olivine 40 vol% with the correction of the Fe/Mg partitioning in equilibrium with Fa_{50}. Compositions of the previous data for possible nakhlite magmas are also plotted as LP89: Longhi and Pan (1989), KML98: Kaneda et al. (1998), NIM: Harvey and McSween 1992b, Trei93: Treiman 1993, and TG01: Treiman and Goodrich 2001. The plot was carried out using oxygen units (Longhi, 1991). The phase boundaries are under the condition of Mg# = 70, $x_{ab} = 0.5$, and $x_{or} = 0.01$, respectively (Longhi 1991). Two plots of mesostasis (m) and AVI under the silica saturated condition were plotted from SiO_2. All other points have olivine saturated compositions. The chemical compositions referred in the figure are given on Tables 1, 4, and 6.

subtraction of possible cumulus phases from the whole rock composition. The calculation to obtain the intercumulus melt composition was carried out using the following mass balance equation for each oxide component.

$$F_{melt}\rho_{melt}w^i_{melt} = \rho_{bulk}w^i_{bulk} - F_{aug,core}\rho_{aug,core}w^i_{aug,core} - kF_{ol}\rho_{ol}w^i_{ol} - F_{Ti-mgt}\rho_{Ti-mgt}w^i_{Ti-mgt} \quad (1)$$

where w^i is concentration of i (= SiO_2, TiO_2, Al_2O_3, FeO, MnO, MgO, CaO, Na_2O, and K_2O in wt%), F is modal fraction of a mineral (0 to 1), and ρ is density. The $w^i_{Ti\text{-}mgt}$ for the components except FeO, Fe_2O_3, and TiO_2 is taken to be zero. The mass and volume balance equations for bulk and mode, respectively, are also satisfied in the following equations:

$$F_{melt}\rho_{melt} = \rho_{bulk} - F_{aug,core}\rho_{aug,core} - kF_{ol}\rho_{ol} - F_{Ti-mgt}\rho_{Ti-mgt} \quad (2)$$

and

$$F_{melt} = 1 - F_{aug,core} - kF_{ol} - F_{Ti-mgt} \quad (3)$$

The averaged bulk composition of the Yamato nakhlites (Table 1) is used for the calculation, and the composition of cumulus olivine was taken to be Fa_{50}. The following modal and density values are used for the calculation to derive the intercumulus melt composition. The modal abundance of all augite phenocrysts is about 77.0 vol% in average (Imae et al. 2003), which is divided into core 61.1% and overgrowth rim 15.9 vol% by using BEI images. The modal abundance of micro-phenocrystic titanomagnetite is 0.6 vol%. The density of the Yamato nakhlites is taken to be 3.29 (for Nakhla, Consolmagno and Britt 1998) and those of augite core,

olivine of Fa_{50} and titanomagnetite are 3.3, 3.8, and 5, respectively.

Then, inserting these values into the equation (1), we obtain following equations for FeO and MgO contents, respectively:

$$F_{melt}\rho_{melt}w_{melt}^{FeO} = \rho_{bulk}w_{bulk}^{FeO} - F_{aug,core}\rho_{aug,core}w_{aug,core}^{FeO} - kF_{ol}\rho_{ol}w_{ol}^{FeO} - F_{Ti-mgt}\rho_{Ti-mgt}w_{Ti-mgt}^{FeO} = (3.29 \times 19.51) - (0.611 \times 3.3 \times 15.03) - (k \times 0.122 \times 3.8 \times 41.74) - (0.006 \times 5 \times 34.58) = 32.83 - 19.35k \quad (4)$$

and

$$F_{melt}\rho_{melt}w_{melt}^{MgO} = \rho_{bulk}w_{bulk}^{MgO} - F_{aug,core}\rho_{aug,core}w_{aug,core}^{MgO} - kF_{ol}\rho_{ol}w_{ol}^{MgO} - F_{Ti-mgt}\rho_{Ti-mgt}w_{Ti-mgt}^{MgO} = (3.29 \times 11.09) - (0.611 \times 3.3 \times 12.39) - (k \times 0.122 \times 3.8 \times 23.42) - (0.006 \times 5 \times 0.49) = 11.50 - 10.85k \quad (5)$$

Then, the partition coefficient of FeO/MgO between core augite and the intercumulus melt is given by

$$K_D^{aug-melt} = \frac{\left(\frac{w_{FeO}}{w_{MgO}}\right)_{aug,core}}{\left(\frac{w_{FeO}}{w_{MgO}}\right)_{melt}} = \frac{\frac{15.03}{12.39}}{\frac{32.83 - 19.35k}{11.50 - 10.85k}} = \quad (6)$$

$$\frac{13.83 - 13.21k}{32.7 - 19.4k}$$

As the Fe/Mg partition coefficient K_D between augite and the intercumulus melt is 0.22 (Grove and Bence 1977), we obtain the fraction of cumulus olivine $k = 0.74$. Because total olivine is 12.2 vol%, 9.0 vol% is cumulus olivine, and 3.2 vol% have grown from the intercumulus melt. The modal abundance and the density of the intercumulus melt are calculated to be 28.6 vol% and 3.07, respectively. The intercumulus melt composition is obtained from Equation 1 for each component and is defined to be that of the Yamato intercumulus melt (YIM), which is listed on Table 4 and is plotted in Fig. 5.

We estimate uncertainties of YIM from the accuracy of modal abundance of core augite, that is, the variation of modal abundance for core augite used for the calculation (61.1 vol%) may have some slight variation. Here we estimate the variation as ±3 vol% at most for core augite. When the mode of augite core is 58.1 vol%, the mode of cumulus olivine of 10.7 vol% is obtained. The calculated intercumulus melt composition (YIM-) is given on Table 4 and plotted in Fig. 5. When the mode of augite core is 64.1 vol%, the mode of cumulus olivine becomes 7.6 vol%, and the calculated intercumulus melt composition (YIM+) is given on Table 4 and plotted in Fig. 5. The obtained data of YIM does not have any large uncertainty.

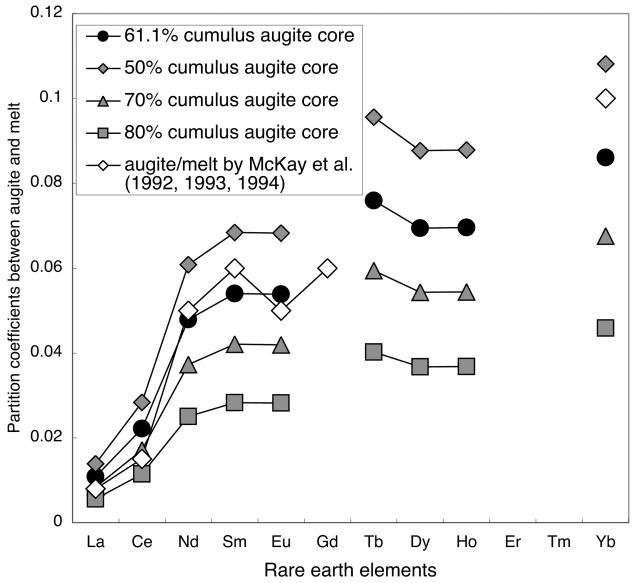

Fig. 6. Partition coefficients of rare earth elements between phenocryst core augite and the calculated intercumulus melts with the experimentally determined reference data (McKay et al. 1992, 1993, 1994). Rare earth elements for core augite in Y-000749 were taken from Wadhwa et al. (2004). Bulk composition for rare earth elements in Y-000749 was taken from Dreibus et al. (2003). The calculated partition coefficients using 61.1 vol% core augite as cumulates are consistent with the data by McKay et al. (1992, 1993, 1994). The modal abundance of 50, 70, and 80 vol% for core augite is also considered for the reference in the figure.

Wadhwa et al. (2004) published the abundance data of rare earth elements of phenocryst core augite in Y-000749, while Dreibus et al. (2003) published the abundance data of rare earth elements for the bulk compositions of the Yamato nakhlites (Y-000593 and Y-000749). Using two sets of data, we carried out the mass balance calculation based on the determined modal abundance of cumulus phases from the major elements, and derived the trace elemental abundance for the Yamato intercumulus melt (Table 8). When we compare the partitioning coefficients for rare earth elements with the experimentally determined partitioning coefficient (McKay et al. 1992, 1993, 1994), we find that two sets of partition coefficients are similar although La and Ce seem to be somewhat higher and Yb is somewhat lower than those of experimental data (McKay et al. 1992, 1993, 1994) (Fig. 6).

Zoning of Phenocrystic Olivine

Olivine phenocrysts have often experienced diffusional modification to form Mg-Fe chemical zoning from magnesian olivine to ferroan olivine. The Fa composition of the phenocrystic olivine coexisting with phenocryst core

Table 4. Chemical compositions (wt%) of the Yamato parent magma (YIM) with references of the parent magmas by Harvey and McSween (1992b), Longhi and Pan (1989), Kaneda et al. (1998), and Treiman and Goodrich (2001).

	YIM–	YIM	YIM+	Longhi and Pan (1989)	Harvey and McSween (1992b)	Treiman (1993)	Kaneda et al. (1998)	Treiman and Goodrich (2001)
SiO_2	48.60	47.26	46.01	49.01	46.27	50.20	49.75	49.8
TiO_2	0.60	0.60	0.60	1.06	3.69	1.00	0.80	0.8
Al_2O_3	4.99	5.12	5.23	2.85	7.66	8.60	5.73	7.5
Fe_2O_3	5.64	5.90	6.13	n.d.	n.d.	n.d.	n.d.	n.d.
FeO	18.14	20.19	22.09	26.23	24.68	19.10	22.96	22.3
MnO	1.15	1.15	1.15	n.d.	n.d.	0.40	0.58	0.5
MgO	3.30	3.66	4.02	5.22	5.42	4.00	4.56	4.6
CaO	13.98	12.42	10.98	13.92	10.04	11.90	12.22	10.4
Na_2O	1.82	1.88	1.93	0.97	1.46	1.20	1.00	1.1
K_2O	0.57	0.59	0.62	0.20	1.20	2.80	1.04	2.4
$H_2O(–)$	0.09	0.09	0.09	n.d.	n.d.	n.d.	n.d.	n.d.
$H_2O(+)$	0.00	0.00	0.00	n.d.	n.d.	n.d.	n.d.	n.d.
P_2O_5	0.65	0.67	0.69	n.d.	n.d.	0.70	0.17	0.6
Cr_2O_3	0.21	0.18	0.15	n.d.	n.d.	0.10	0.05	0.1
FeS	0.28	0.29	0.30	n.d.	n.d.	n.d.	n.d.	n.d.
NiO	n.d.	n.d.	n.d.	n.d.	n.d.	0.00	n.d.	n.d.
Total	100.00	100.00	100.00	99.46	100.42	99.20	98.64	99.40
Norm (oxygen unit)								
Wo	29.98	26.77	23.75	29.40	19.03	25.73	24.46	22.00
Opx	33.46	28.09	23.09	51.95	32.28	34.20	53.62	41.65
Pl	24.51	25.52	26.39	13.66	31.12	28.69	21.17	24.91
Ol	12.06	19.62	26.78	4.99	17.56	11.38	0.75	11.44
Norm (oxygen unit)								
Pl	24.51	25.52	26.39	13.66	31.12	10.40	21.17	24.91
Wo	29.98	26.77	23.75	29.40	19.03	33.67	24.46	22.00
Ol	34.00	38.34	42.00	39.63	39.08	33.55	36.49	39.20
Qtz	11.00	9.36	7.70	17.32	10.76	22.38	17.88	13.88
$K_D^{\text{aug core-melt}}$		0.22		0.24	0.27	0.25	0.24	0.25

Table 5. Modal abundance (vol%) of constituting phases in rounded vitrophyric inclusions (RVIs).

	Density	RVI-1	RVI-2	RVI-3	RVI-4	RVI-5
Augite	3.4	62.6	63.3	71.8	71.1	58.6
Glass	2.6	37.4	36.7	28.2	24.9	37.3
Titanomagnetite	5	0	0	0	4	4.1
Calculated density		3.1	3.2	3.2	3.3	3.2

augite is obtained from the Fe/Mg partition coefficient. The partition coefficient of FeO/MgO, $K_D^{cpx\text{-}liquid}$, between augite and liquid is 0.22 (Grove and Bence 1977), and the partition coefficient of FeO/MgO, $K_D^{ol\text{-}liquid}$, between olivine and liquid is 0.33 (Longhi et al. 1978). Combining these two coefficients, $K_D^{cpx\text{-}ol}$ between augite and olivine is 0.67 (=0.22/0.33). The calculation indicates that the chemical composition of the olivine in equilibrium with phenocryst core augite ($En_{36}Fs_{25}Wo_{39}$; Mg# = 59) should have Mg# = 50. The magnesian olivine (Fa_{50}) does not occur in the Yamato nakhlites. Instead, more ferroan olivines occur with normal compositional zoning. The zoning of olivine must have been produced by cation diffusion in cumulates to change the magnesian olivine (Fa_{50}) to more ferroan ones.

Trapped Melt Composition Estimated from Vitrophyric Inclusions in Olivine Phenocrysts

Rounded vitrophyric inclusions are magmatic inclusions in olivine phenocrysts and might be related to the magma from which the nakhlites crystallized (Harvey and McSween 1992b; Treiman 1993). Four rounded vitrophyric inclusions in the first thin section (Y-000802; RVI-1-4), three small ones (~20 μm) in the second thin section (Y-000593) and one inclusion in the third thin section (Y-000749; RVI-5) (Fig. 1g) were identified. Among them, rounded vitrophyric inclusions in the second thin section (Y-000593) were small and not used for the following analyses. The Na_2O contents of glass in the first thin section (Y-000802) seem to be depleted, and K_2O in

Table 6. Candidates of corrected trapped magma compositions (wt%) obtained from a rounded vitrophyric inclusion (RVI-5) by addition of the wall olivine surrounding the magmatic inclusion.

	RVI-5[a]	RVI-5'[b]	A[c]	B[d]	C[e]	D[f]
SiO_2	50.08	49.66	47.19	44.88	42.45	40.04
TiO_2	2.34	2.32	2.02	1.74	1.46	1.21
Al_2O_3	10.48	10.39	9.04	7.78	6.56	5.40
FeO	16.53	18.58	23.76	28.62	33.48	38.18
MnO	0.3	0.30	0.26	0.22	0.19	0.15
MgO	4.59	3.44	4.40	5.30	6.20	7.07
CaO	12.32	12.22	10.63	9.15	7.71	6.35
Na_2O	2.46	2.44	2.12	1.83	1.54	1.27
K_2O	0.64	0.63	0.55	0.48	0.40	0.33
Cr_2O_3	0.02	0.02	0.02	0.02	0.01	0.01
Total	99.76	100.00	100.00	100.00	100.00	100.01
Norm (oxygen unit)						
Wo	20.02	19.99	17.71	15.49	13.29	11.14
Opx	29.81	29.41	25.03	20.75	15.34	9.27
Pl	44.34	44.29	39.23	34.32	29.44	24.69
Ol	5.83	6.3	18.03	29.44	41.93	54.9
Norm (oxygen unit)						
Pl	44.34	44.29	39.23	34.32	29.44	24.69
Wo	20.02	19.99	17.71	15.49	13.29	11.14
Ol	25.70	25.91	34.72	43.27	52.15	61.08
Qtz	9.94	9.81	8.34	6.92	5.11	3.09

[a]Bulk composition of a rounded vitrophyric inclusion (RVI-1) is obtained from the modal abundances of the inclusion and the compositions and densities of the constituent minerals (Table 4).
[b]Fe/Mg corrected of RVI-5 in equilibrium with Fa_{50}.
[c]RVI-5 and wall olivine 10 vol% with the correction of Fe/Mg partioning in equilibrium with Fa_{50}.
[d]RVI-5 and wall olivine 20 vol% with the correction of Fe/Mg partioning in equilibrium with Fa_{50}.
[e]RVI-5 and wall olivine 30 vol% with the correction of Fe/Mg partioning in equilibrium with Fa_{50}.
[f]RVI-5 and wall olivine 40 vol% with the correction of Fe/Mg partioning in equilibrium with Fa_{50}.

Table 7. Modal abundance (vol%) of constituting phases in inclusions in augite phenocrysts.

	Density	Incl-3	Incl-4	Incl-7	Incl-8
Augite halo	3.4	72	60	48	65
Glass	2.6	26	31	40	28
Titanomagnetite	5	3	9	13	7
Calcurated density		3.3	3.3	3.3	3.3

these inclusions are higher than Na_2O (Table 3). This may be due to Martian or terrestrial weathering of glass. RVI-5 in the third thin section (Y-000749) has higher Na_2O contents than K_2O (Table 3) and is used in the following discussion. Bulk composition of RVI-5 in Y-000749 was calculated from the modal abundance of augite, glass, and titanomagnetite (Table 5). The densities are taken to be 3.4 for augite, 2.6 for glass, and 5 for titanomagnetite as shown in Table 5. The bulk composition for RVI-5 is shown in Table 6 and the compositions of constituent phases are shown in Table 2 and Table 3.

RVI-5 must have crystallized much wall olivine during the early stage crystallization of the inclusion. Therefore, the wall olivines must be added to rounded vitrophyric inclusion to obtain the initial trapped melt. The added olivine is tentatively taken to be Fa_{65} (density 3.8), which is just surrounding the RVI-5. The candidates of apparent trapped melts are obtained by addition of 10, 20, 30, and 40 vol% of olivine (Table 6).

The initial trapped melt for RVI-5 may be assumed to have equilibrated with Fa_{50} olivine. We corrected the Mg# of the candidates of apparent trapped melts to obtain the true trapped melts keeping the total molar number of Mg and Fe. That is, 4.59 wt% MgO and 16.53 wt% FeO for the apparent trapped melt (Table 6) were corrected to be 3.44 wt% and 18.58 wt%, respectively. The calculated bulk chemical compositions normalized to 100 wt% are shown in Table 6, and are plotted in Fig. 5, which shows that the trapped melts for the magmatic inclusions in olivine corresponds to moderately fractionated melts. The compositions with 20–30 vol% olivine (B and C) are on the way of the arrow from YIM to mesostasis in Fig. 5, and seem to be appropriate estimation of trapped melt compositions.

Angular vitrophyric inclusions (Fig. 1h) consist of fine-

Table 8. The intercumulus melt composition of Y-000749, the partition coefficient of rare earth elements between phenocryst augite core and the intercumulus melt, and the reference data.

Rare earth elements	Bulk of Y-000749[a] (ppm)	Augite phenocryst core of Y-000749[b] (ppm)	Calculated intercumulus melt composition (ppm)	Augite core/Intercumulus melt
La	2.73	0.075	6.98	0.0107
Ce	7.05	0.39	17.71	0.0220
Nd	4.26	0.49	10.29	0.0476
Sm	1.09	0.14	2.61	0.0536
Eu	0.32	0.041	0.76	0.0540
Gd	–	0.16	–	–
Tb	0.16	0.028	0.37	0.0754
Dy	0.99	0.16	2.32	0.0690
Ho	0.21	0.034	0.49	0.0691
Er	–	0.09	–	–
Tm	–	0.0092	–	–
Yb	0.46	0.090	1.04	0.0866

[a]Dreibus et al. (2003).
[b]Wadhwa et al. (2004).

grained materials (Table 1 and Fig. 5) and have melt veins connecting with mesostasis, suggesting that the angular vitrophyric inclusions were produced by intrusion of mesostasis melt during the final stage of crystallization. Thus, angular vitrophyric inclusions do not represent the early-stage magma, but a late-stage fractionated melt.

Trapped Melt Composition Estimated from Glass Inclusion in Augite Phenocryst Cores

Many glass inclusions occur in augite phenocryst cores in close association with titanomagnetites and ferroan augite halos, and they are magmatic inclusions (Fig. 1c). We calculated the bulk compositions using the modal abundances and the chemical compositions of glass, titanomagnetite and halo from four large inclusions in Y-000749, 1-3 (Table 7). The average composition of the four inclusions is shown in Table 1. The composition is similar to the intercumulus melt composition (YIM).

Mesostasis Formation

The crystallization trend of fractionated melt is shown in the pseudo ternary phase diagram (Fig. 5). Augite phenocrysts crystallized from the original magma together with olivines and accumulated on the floor of the magma chamber to form the Yamato nakhlites.

The intercumulus melt (YIM) between cumulate phenocrysts rapidly cooled to form the inner rim surrounding augite phenocrysts. The fractionated melt went deeply into the plagioclase stability field, resulting in the composition of mesostasis, and the melt trend is indicated as thick arrows in Fig. 5. Then, the mesostasis melt nucleated plagioclase. Too much crystallization of plagioclase caused the residual melt to go into the low Ca-pyroxene stability field (Fig. 5) and precipitated the outer rims of augite and mesostasis low Ca-pyroxene. Therefore, pyroxenes in the mesostasis and the outer rims of augite are depleted in Ca, and are mainly pigeonite or subcalcic augites (Table 2).

The cooling rates of four nakhlites were determined from Fe-Mg chemical zoning in olivine by Mikouchi and Miyamoto (2002). They are 0.015 °C/hr for Lafayette, 0.04 °C/hr for Nakhla, 0.085 °C/hr for Governador Valadares, and 2.2 °C/hr for NWA 817. These cooling rates suggest that nakhlites have formed under rapid cooling conditions such as lava flows or sills, and the rates have produced the fine-grained texture of the mesostasis in nakhlites. The zoning patterns of olivines in the Yamato nakhlites are intermediate between those in Nakhla and NWA 817 (Mikouchi et al. 2003; Imae et al. 2003), suggesting that the cooling rate of the Yamato nakhlites may be 0.04–2.2 °C/hr.

Formation of Exsolution Lamellae, Symplectites, and Augite-Magnetite Aggregates in Olivine Phenocrysts, and Ilmenie Lamellae from Titanomagnetites

The exsolution lamellae, symplectites, and augite-magnetite aggregates occur within olivines in the Yamato nakhlites, and they may have formed under a slow cooling condition. The exsolution lamellae in Martian meteorites have been reported in olivines in Nakhla and Governador Valadares (Mikouchi et al. 2000; Mikouchi and Miyamoto 1998), NWA 998 (Irving et al. 2002; Bridges et al. 2004) and the Yamato nakhlites (Imae et al. 2003; Mikouchi et al. 2003; Bridges et al. 2004), although they have never been reported in Lafayette and NWA 817. Similar lamellar structures consisting of magnetite and clinopyroxene in olivines have been reported in terrestrial rocks such as the Rhum Intrusions, Scotland (Putnis 1979; Putnis and McConnell 1980; Moseley 1984). The exsolution lamellae in terrestrial olivines seem to

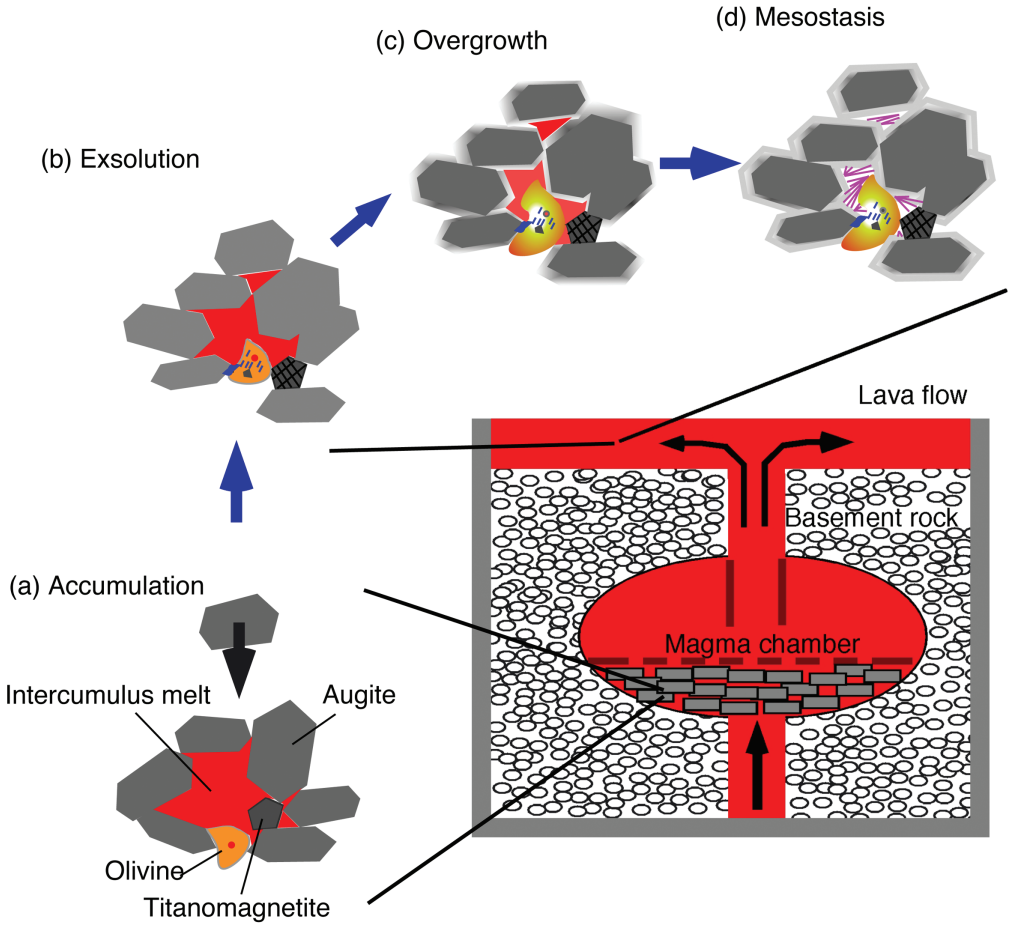

Fig. 7. A schematic illustration showing the accumulation of crystals in a magma chamber and the crystallization after the intrusion from magma chamber to form lava flow formed nakhlites with the crystallization sequence for the Yamato nakhlites. a) Accumulation of three phenocrysts of augite cores, olivine cores, and titanomagnetites on the floor in the magma chamber. Olivine grains trapped melt inclusions. The chemical compositions of olivines and augites were Fa_{50} and $En_{36}Fs_{25}Wo_{39}$, respectively. b) Augite-magnetite aggregates, symplectites and lamellae exsolved in olivine core. c) Growth of olivine phenocryst and augite inner rims with diffusional modification for Mg-Fe zoning. d) Growth of outer rims surrounding augite inner rims and mesostasis crystallization mostly consisting of plagioclase.

accompany oxidation (Putnis 1979; Putnis and McConnell 1980). These exsolution features have formed by nucleation and growth of lamellae phases in association with defect structures such as dislocations in olivine crystals (Putnis and McConnell 1980). While, Moseley (1984) discussed the formation of lamellae consisting of two phases based on an assumption that ferric irons initially existed in olivine. On the other hand, in olivine phenocryst in Y-000593, Bridges et al. (2004) recently found exsolution lamellae mainly consisting of stoichiometric Ca-rich olivine with CaO = 9–16 wt% and suggested that the lamellae consisting of magnetite and augite were formed by the decomposition of the Ca-rich olivine lamellae.

The augite composition in lamellae in Y-000593 (Mg# = 63) was obtained by Noguchi et al. (2003), and it is similar in composition with augite phenocryst cores (Mg# = 59) within an experimental error. Therefore the Mg and Fe atoms in lamellae augite would be partitioned with the host olivine under an equilibrium condition, suggesting that the exsolution to produce lamellae in the Yamato nakhlites may have already started to form at high temperature before the final diffusional modification of olivine phenocrysts in the late stage of crystallization.

Judging from the texture of Fig. 1j, lamellae formed after the symplectite formation, and symplectites in olivine formed on augite-magnetite aggregates. Therefore the formation sequence is augite-magnetite aggregates, symplectites and lamellae in this order. The precursor of the augite-magnetite lamellae could be the CaO-rich olivine lamellae which were proposed by Bridges et al. (2004), but it is not clear whether Bridges' scenario is correct or not.

As already stated, symplectites commonly occur at augite-olivine boundaries (Figs. 1f and k). The Mg# =60 of symplectite augites at the olivine-augite boundaries is similar to those of augite phenocryst cores. Symplectites may have formed after accumulation of augite and olivine phenocrysts and before rapid cooling to form augite rims and mesostasis.

Ilmenite exsolution lamellae are common in

titanomagnetites of the Yamato nakhlites, and occur in all known nakhlites. These are also common in terrestrial igneous rocks, and are thought to result from oxidation of magnetite-ulvöspinel solid solutions (e.g., Buddington and Lindsley 1964; Spencer and Lindsley 1981; Putnis and McConnell 1980).

SUMMARY: FORMATIONAL SCENARIO

We present a formational scenario of the Yamato nakhlites in Fig. 7. Phenocryst core augite, phenocryst core olivine and microphenocryst titanomagnetite crystallized at high magmatic temperature, and accumulation at magma chamber floors took place (Fig. 7a). The cumulates intruded upward to the surface with the interstitial melt. Augite-magnetite aggregates, symplectites and exsolution lamellae in olivines may have produced at this stage under a slow cooling condition (Fig. 7b). With the overgrowth of olivine phenocryst, the inner rim surrounding the augite phenocryst core formed by the crystallization of the intercumulus melt. The diffusional modification to produce compositional zonation of olivine was caused by Mg-Fe diffusion under a rapid cooling condition such as lava flow or sill (Fig. 7c). Subsequently, the outer rim formed with crystallization of residual melt to form plagioclase of mesostasis (Fig. 7d).

CONCLUSIONS

1. Subtraction of cumulus phases of phenocryst core augite, phenocryst core olivine, and microphenocryst titanomagnetites from the bulk composition gives the composition of primary intercumulus melt defined to be the Yamato intercumulus melt (YIM).
2. Three types of inclusions in olivine phenocrysts were identified. Angular vitrophyric inclusions are derived from late-stage fractionated interstitial melts. Rounded vitrophyric inclusion (RVI-5) may represent the middle-stage melt.
3. Trapped melt composition was also estimated from inclusions consisting of Si-rich glass, titanomagnetites and ferroan augite halos in phenocryst core augites, and it is similar to YIM.
4. Augite-magnetite aggregates, symplectites and lamellae in olivine phenocrysts may have formed on Martian surface after the accumulation of cumulus minerals. Martian surface caused the interstitial melt to rapidly crystallize mesostasis, olivine and augite rims.

Acknowledgments–We are grateful to Drs. A. Treiman, R. Harvey, J. Bridges, A. Irving and an anonymous referee for their critical and constructive reviews, and to the members of the 41st Japanese Antarctic Research Expedition for their support of the meteorite search near the Yamato mountains. We are also grateful to Drs. T. Noguchi and T. Hokada for discussions, and are grateful to Dr. Paul Buchanan for his reading of the manuscript. This research is partly supported by a Grant-in-Aid of the Japanese Ministry of Education, Science, and Culture (15540463).

Editorial Handling— Dr. Allan Treiman

REFERENCES

Bridges J. C., Warren P. H., and Lee M. R. 2004. Olivine decomposition features in the Y-000593 and NWA 998 nakhlites (abstract). *Meteoritics & Planetary Science* 39:A18.

Buddington A. F. and Lindsley D. H. 1964. Iron-titanium oxide minerals and synthetic equivalents. *Journal of Petrology* 5:310–357.

Bunch T. E. and Reid A. M. 1975. The nakhlites Part I: Petrography and mineral chemistry. *Meteoritics* 10:303–315.

Burrangato F., Cavaretta G., and Funiciello R. 1975. The new Brazilian achondrite of Governador Valadares (Minas Gerais). *Meteoritics* 10:374–375.

Consolmagno G. J. and Britt D. T. 1998. The density and porosity of meteorites from the Vatican collection. *Meteoritics & Planetary Science* 33:1231–1241.

Dreibus G., Huisl W., Spettel B., and Haubold R. 2003. Comparison of the chemistry of Y-000593 and Y-000749 with other nakhlites (abstract #1586). 34th Lunar and Planetary Science Conference. CD-ROM.

Friedman Lentz R. C., Taylor G. J., and Treiman A. H. 1999. Formation of a Martian pyroxenite: A comparative study of the nakhlite meteorites and Theo's Flow. *Meteoritics & Planetary Science* 34:919–932.

Greshake A., Stephen T., and Rost D. 1998. Symplectic exsolutions in olivine from the Martian meteorite Chassigny: Evidence for slow cooling under highly oxidizing conditions (abstract #1069). 29th Lunar and Planetary Science Conference. CD-ROM.

Grove T. L. and Bence A. E. 1977. Experimental study of pyroxene-liquid interaction in quartz-normative basalt 15597. Proceedings, 8th Lunar Science Conference. pp. 1549–1579.

Harvey R. P. and McSween H. Y. Jr. 1992a. Petrogenesis of the nakhlite meteorites: Evidence from cumulate mineral zoning. *Geochimica et Cosmochimica Acta* 56:1655–1663.

Harvey R. P. and McSween H. Y. Jr. 1992b. The parent magma of the nakhlite meteorites: Clues from melt inclusions. *Earth and Planetary Science Letters* 111:467–482.

Ikeda Y. 1980. Petrology of Allan Hills 764 chondrite (LL3). *Memoirs of National Institute of Polar Research* 17:50–82.

Imae N., Ikeda Y., Shinoda K., Kojima H., and Iwata N. 2003. Yamato nakhlites: Petrography and mineralogy. *Antarctic Meteorite Research* 16:13–33.

Irving A. J., Kuehner S. M., Rumble D. III, Carlson R.W., Hupé A. C., and Hupé G. M. 2002. Petrology and isotopic composition of orthopyroxene-bearing nakhlite NWA 998 (abstract). *Meteoritics & Planetary Science* 37:A70.

Kaneda K., McKay G., and Le L. 1998. Synthetic and natural pyroxenes: A close match at last (abstract #1620). 29th Lunar and Planetary Science Conference. CD-ROM.

Longhi J., Walker D., and Hays J. F. 1978. The distribution of Fe and Mg between olivine and lunar basaltic liquids. *Geochimica et Cosmochimica Acta* 42:1545–1558.

Longhi J. and Pan V. 1989. The parent magmas of the SNC meteorites. Proceedings, 19th Lunar and Planetary Science Conference. pp. 451–464.

Longhi J. 1991. Comparative liquidus equilibria of hyperthene-

normative basalts at low pressure. *American Mineralogist* 76: 785–800.

McKay G., Le L., and Wagstaff J. 1992. REE partition coefficients for the Nakhla parent melt (abstract). 23rd Lunar and Planetary Science Conference. pp. 889–890.

McKay G., Le L., and Wagstaff J. 1993. The Nakhla parent melt: REE partition coefficients and clues to major element composition (abstract). 24th Lunar and Planetary Science Conference. pp. 965–966.

McKay G., Le L., and Wagstaff J. 1994. Synthetic and natural Nakhla pyroxenes: Parent melt composition and REE partition coefficients (abstaract). 25th Lunar and Planetary Science Conference. pp. 883–884.

McKay G. and Schwandt C. 2005. Mineralogy and petrology of new Antarctic nakhlite MIL 03346 (abstract #2351). 36th Lunar and Planetary Science Conference. CD-ROM.

McSween H. Y., Jr. 1985. SNC meteorites: Clues to Martian petrologic evolution? *Review of Geophysics* 23:391–416.

Mikouchi T. and Miyamoto M. 1998. Pyroxene and olivine microstructures in nakhlite Martian meteorites: Implication for their thermal history (abstract #1574). 29th Lunar and Planetary Science Conference. CD-ROM.

Mikouchi T., Yamada I., and Miyamoto M. 2000. Symplectic exsolution in olivine from the Nakhla Martian meteorite. *Meteoritics & Planetary Science* 35:937–942.

Mikouchi T. and Miyamoto M. 2002. Comparative cooling rates of nakhlites as inferred from iron-magnesium and calcium zoning of olivines (abstract #1343). 33rd Lunar and Planetary Science Conference. CD-ROM.

Mikouchi T., Koizumi E., Monkawa A., Ueda Y., and Miyamoto M. 2003. Mineralogy and petrology of Yamato-000593: Comparison with other Martian nakhlite meteorites. *Antarctic Meteorite Research* 16: 34–57.

Misawa K., Kojima H., Imae N., and Nakamura N. 2003. The Yamato nakhlite consortium. *Antarctic Meteorite Research* 16:1–12.

Moseley D. 1984. Symplectic exsolution in olivine. *American Mineralogist* 69: 139–153.

Noguchi T., Imae N., Misawa K., and Nakamura T. 2003. Mineralogy of "iddingsite" and symplectite in Y-000593 and Y-000749: Implication for their post-crystallization and aqueous alteration (abstract). International Symposium Evolution of Solar System Materials: A New Perspective from Antarctic Meteorites. pp. 105–106.

Prior G. T. 1912. The meteoritic stones of El Nakhla El Baharia (Egypt). *Mineralogical Magazine* 16:274–281.

Putnis A. 1979. Electron petrography of high-temperature oxidation in olivine from the Rhum Layered Intrusion. *Mineralogical Magazine* 43:293–296.

Putnis A. and McConnell J. D. C. 1980. *Principles of mineral behaviour*. Oxford: Blackwell Scientific Publications. 257 p.

Sautter V., Barrat J. A., Jambon A., Lorand J. P., Gillet P., Javoy M., Joron J. L., and Lesourd M. 2002. A new Martian meteorite from Morocco: The nakhlite Northwest Africa 817. *Earth and Planetary Science Letters* 195:223–238.

Spencer K. J. and Lindsley D. H. 1981. A solution model for coexisting iron-titanium oxides. *American Mineralogist* 66: 1189–1201.

Treiman A. H. 1986. The parental magma of the Nakhla achondrite: Ultrabasis volcanism on the shergottite parent body. *Geochimica et Cosmochimica Acta* 50:1061–1070.

Treiman A. H. 1990. Complex petrogenesis of the Nakhla (SNC) meteorite: Evidence from petrography and mineral chemistry. Proceedings, 20th Lunar and Planetary Science Conference. pp. 273–280.

Treiman A. H. 1993. The parent magma of the Nakhla (SNC) meteorite, inferred from magmatic inclusions. *Geochimica et Cosmochimica Acta* 57:4753–4767.

Treiman A. H. and Goodrich C. A. 2001. A parent magma for the Nakhla Martian meteorite: Reconciliation of estimates from 1bar-experiments, magmatic inclusions in olivine, and magmatic inclusions in augites (abstract #1107). 32nd Lunar and Planetary Science Conference. CD-ROM.

Varela M. E., Kurat G., and Clocchiatti R. 2001. Glass-bearing inclusions in Nakhla (SNC meteorite) augite: Heterogeneously trapped phases. *Mineralogy and Petrology* 71:155–172.

Wadhwa M., Crozaz G., and Barrat J. 2004. Trace element distributions in the Yamato-000593/-000749, NWA 817, and NWA 998 nakhlites: Implication for their petrogenesis and mantle source on Mars. *Antarctic Meteorite Research* 17:97–116.